01 Jun 2014

The Capacity of Hydrous Fluids to Transport and Fractionate Incompatible Elements and Metals within the Earth's Mantle

John Adam

Marek Locmelis
Missouri University of Science and Technology, locmelism@mst.edu

Juan Carlos Afonso

Tracy Rushmer

et. al. For a complete list of authors, see https://scholarsmine.mst.edu/geosci_geo_peteng_facwork/738

Recommended Citation

J. Adam et al., "The Capacity of Hydrous Fluids to Transport and Fractionate Incompatible Elements and Metals within the Earth's Mantle," *Geochemistry, Geophysics, Geosystems*, vol. 15, no. 6, pp. 2241-2253, Blackwell Publishing Ltd, Jun 2014.
The definitive version is available at https://doi.org/10.1002/2013GC005199

AGU PUBLICATIONS

Geochemistry, Geophysics, Geosystems

RESEARCH ARTICLE

10.1002/2013GC005199

Key Points:
- Aqueous fluids mantle fluids were simulated experimentally
- Aqueous fluids play a distinct role in chemical differentiation of the Earth

Supporting Information:
- Figures S1–S12
- Tables S1–S2
- Read Me

Correspondence to:
J. Adam,
john.adam@mq.edu.au

Citation:
J. Adam, M. Locmelis, J. C. Afonso, T. Rushmer, and M. L. Fiorentini (2014), The capacity of hydrous fluids to transport and fractionate incompatible elements and metals within the Earth's mantle, *Geochem. Geophys. Geosyst.*, *15*, 2241–2253, doi:10.1002/2013GC005199.

Received 17 DEC 2013
Accepted 22 MAR 2014
Accepted article online 26 MAR 2014
Published online 5 JUN 2014

The capacity of hydrous fluids to transport and fractionate incompatible elements and metals within the Earth's mantle

John Adam[1], Marek Locmelis[2], Juan Carlos Afonso[1], Tracy Rushmer[1], and Marco L. Fiorentini[2]

[1]Australian Research Council Centre of Excellence for Core to Crust Fluid Systems/GEMOC, Department of Earth and Planetary Sciences, Macquarie University, New South Wales, Australia, [2]Centre for Exploration Targeting, Australian Research Council Centre of Excellence for Core to Crust Fluid Systems, School of Earth and Environment, The University of Western Australia, Crawley, Western Australia, Australia

Abstract Both silicate melts and aqueous fluids are thought to play critical roles in the chemical differentiation of the Earth's crust and mantle. Yet their relative effects are poorly constrained. We have addressed this issue by measuring partition coefficients for 50 trace and minor elements in experimentally produced aqueous fluids, coexisting basanite melts, and peridotite minerals. The experiments were conducted at 1.0–4.0 GPa and 950–1200°C in single capsules containing (either 40 or 50 wt %) H_2O and trace element-enriched basanite glass. This allowed run products to be easily identified and analyzed by a combination of electron microprobe and LAM-ICP-MS. Fluid and melt compositions were reconstructed from mass balances and published solubility data for H_2O in silicate melts. Relative to the basanite melt, the solutes from H_2O-fluids are enriched in SiO_2, alkalis, Ba, and Pb, but depleted in FeO, MgO, CaO, and REE. With increasing pressure, the mutual solubility of fluids and melts increases rapidly with complete miscibility between H_2O and basanitic melts occurring between 3.0 and 4.0 GPa at 1100°C. Although LREE are favored over HREE in the fluid phase, they are less soluble than the HFSE (Nb, Ta, Zr, Hf, and Ti). Thus, the relative depletions of HFSE that are characteristic of arc magmas must be due to a residual phase that concentrates HFSE (e.g., rutile). Otherwise, H_2O-fluids have the capacity to impart many of the geochemical characteristics that distinguish some rocks and melts from the deep mantle lithosphere (e.g., MARID and lamproites).

1. Introduction

Information about the compositions of hydrous fluids in equilibrium with mantle rocks is important for the solution of a number of significant petrogenetic problems. These include: the origins of arc volcanism [*Green*, 1973; *Saunders and Tarney*, 1979; *Tatsumi et al.*, 1986; *Turner et al.*, 1997; *Brenan et al.*, 1998; *Johnson and Plank*, 1999]; incompatible element enrichments in lithospheric mantle xenoliths [*Nielson and Noller*, 1987; *O'Reilly and Griffin*, 1988; *Loyd and Bailey*, 1975; *Bailey*, 1982; *Bodinier et al.*, 1996; *Melzer et al.*, 1998]; and the mechanisms by which economically important metals are transferred from the mantle to the continental crust [*Ballhaus et al.*, 1994; *Fiorentini and Beresford*, 2008]. However, for a number of reasons, this has been a technically difficult issue to address experimentally. Partially, this is because of the practical impossibility of preserving aqueous fluids produced under simulated mantle conditions once they have been quenched to room temperature and pressure. After quenching, most of the dissolved solids originally contained in the fluids are precipitated. The precipitated solids are both heterogeneous and physically fragile making their collection and analysis a challenging aspect of experimental design, as is the estimation of total solute concentrations in the original fluids. Various stratagems have been attempted for both of these problems.

One strategy is the use of double capsules whereby a permeable inner capsule (containing the solid starting material) is placed inside a larger H_2O-filled outer capsule [e.g., *Ayers and Eggler*, 1995; *Ayers et al.*, 1997; *Green and Adam*, 2003]. This allows solutes from the fluid phase to be trapped between the walls of the inner and outer capsules; from there, they can then be conveniently collected, chemically analyzed, and weighed. By comparing the weight of the recovered solute with the mass of H_2O released from capsules on drying, a minimum estimate of solute concentrations in the original fluids can be obtained [see *Ayers and Eggler*, 1995]. A more direct approach has been to equilibrate crystals and/or melts with H_2O in single capsules and then (after experiments are finished) to either physically [e.g., *Brenan et al.*, 1995a, 1995b; *Adam et al.*, 1997] or chemically [e.g., *Ayers and Watson*, 1993; *Keppler*, 1996] separate solutes from other phases. Fluid inclusions in crystals have also been used to trap bulk fluid samples [e.g., *Ballhaus et al.*, 1994; *Adam* *et al*., 1997]. A more recent method has been to trap fluids within the interstices of diamond aggregates and then to analyze these by laser ablation microprobe and inductively coupled plasma mass spectrometry (LAM-ICP-MS) [e.g., *Stalder et al*., 1998; *Kessel et al*., 2004, 2005a, 2005b].

All of the described strategies have their various advantages and disadvantages. Generally, they have also made the most of the analytical technologies available at the time of their use. Thus, only the more recent studies have benefited from the resolution, sensitivity, and multielement capabilities of the laser microprobe and ICP-MS [e.g., *Stalder et al*., 1998; *Green and Adam*, 2003; *Kessel et al*., 2005b]. Experiments that make use of traps to isolate the fluid phase have the advantage that the fluid phase (or its precipitated solute) can be more conveniently collected and analyzed in bulk. But they also lessen the degree of contact between the fluid phase and coexisting crystals and/or melts. Thus, it is more difficult to ensure equilibrium between trapped fluids and other phases. Experiments that allow direct contact between fluids and solids have the alternative problem that it is difficult to separate precipitated solutes from other run products at the end of experiments. This can be overcome by using large fluid to solid ratios during experiments that facilitate physical separation after experiments [e.g., *Brenan et al*., 1995a, 1995b]. But this also ensures that the crystal phases originally present during experiments have a limited capacity to buffer fluid compositions (these must be either left to chance or predetermined). Thus, the fluids produced during experiments may be significantly different from their natural analogues which are buffered by polymineralic crystal assemblages and large solid to fluid ratios. Another approach that mitigates this problem is to use smaller fluid ratios and to equilibrate fluids with natural silicate melts (whose compositions have previously been determined by equilibrium with complex natural mineral assemblages). Provided that mineral/melt partition coefficients are available for the same melts, fluid/mineral partition coefficients can also be determined. This strategy was used by *Keppler* [1996] to determine fluid/mineral partition coefficients for clinopyroxene. A further advantage of this approach is that it is relatively easy to equilibrate two fluid phases (aqueous fluid and hydrous silicate melt). Hydrous silicate melts are also a more efficient flux of equilibrium crystal growth than are low-density aqueous fluids.

In this present study, we have used the strategy of *Keppler* [1996] to take advantage of a large and self-consistent mineral/melt partition coefficient set for peridotite minerals and hydrous nepheline basanite melts. These partition coefficients were obtained during an earlier experimental study by *Adam and Green* [2006]. The basanite used by *Adam and Green* [2006] was also the subject of a liquidus phase equilibrium study by *Adam* [1990] who determined conditions of multiple saturation with garnet lherzolite at $\sim$2.7 GPa and 1200°C with 4.5 wt % of dissolved H_2O and 2.0 wt % of dissolved CO_2. Although doped with trace elements for experiments, the basanite is natural and has a primitive composition consistent with a direct mantle origin [*Adam and Green*, 2011]. Geochemical evidence also suggests formation by a relatively small degree of peridotite melting [*Adam and Green*, 2011]. Thus, the partitioning data obtained in this study is specifically relevant to aqueous fluids in equilibrium with fertile peridotite under near-solidus mantle conditions. They complement earlier experimental studies by *Schneider and Eggler* [1986] and *Ayers et al*. [1997], but provide data for a more comprehensive range of trace and minor elements (50). The new data also allow for a more direct comparison of the effects of migrating aqueous fluids versus hydrous silicate melts on trace element mobility within the Earth's mantle. In addition, by conducting experiments across a broad range of conditions (1.0–4.0 GPa and 950–1200°C), we are able to describe more fully the effects of changing pressure and temperature on the transport capacities of aqueous fluids in the peridotitic mantle.

2. Experimental and Analytical Methods

2.1. Experimental Rational

The central principle of our experimental approach is that if a silicate melt is in equilibrium with peridotite, any other phase in equilibrium with that melt (including a hydrous fluid) will also be in equilibrium with peridotite. Thus,

$$D_Z^{\text{fluid/peridotite}} = D_Z^{\text{fluid/melt}} / D_Z^{\text{peridotite/melt}} \tag{1}$$

(where D is the Nernst partition coefficient and Z is the element of interest).

Although none of the H_2O-saturated experiments on UT-70489 exactly reproduce the original conditions of lherzolite equilibrium (as determined by *Adam* [1990]), and some depart from it fairly widely, the effect of this on our results is unlikely to be profound. This is because H_2O-rich melts of broadly "basaltic" character (and thus akin to the basanite) can exist in equilibrium with peridotite over a broad range of conditions, including those produced in most of our experiments [see *Green*, 1976; *Hirose and Kawamoto*, 1995]. Consistent with this, all but one of our experiments crystallized olivine (an essential peridotite phase). One (subsolidus) experiment also crystallized a complete amphibole-mica-lherzolite assemblage.

2.2. Starting Materials

Experiments were performed on mixtures of a trace element-enriched basanite glass and water. The proportions used were either 3:2 or 1:1. The basanite glass was prepared from a natural basanite (UT-70489) after it had been doped with an assortment of synthetic trace elements (Table S1). In all cases, the total mass of starting materials was 20 mg with the proportions of H_2O and glass adjusted to equal this amount. To ensure this, a careful check of weights was kept at all stages of capsule preparation and also after experiments.

2.3. Experimental Apparatus and Methods

All experiments were performed in end-loaded piston-cylinder apparatus of the type described by *Boyd and England* [1960]. Furnace assemblies were of 1.27 mm diameter with talc outer sleeves, Pyrex® inner sleeves, graphite heaters, and air-fired boron-nitride inserts. Thermocouples were of *S* type (Pt-$Pt_{90}Rh_{10}$) and no attempt was made to correct for the effect of pressure on emf. Experiments were run using a cold piston-in technique with a minus 10% correction for the effects of friction on measured pressures [see *Green et al*., 1966]. The capsules used in experiments were made from a variety of precious metals and their alloys. These included: Au, $Ag_{70}Pd_{30}$, and $Au_{80}Pd_{20}$. Distilled H_2O was added to capsules using a graduated microsyringe. Although no attempt was made to reverse experiments, previous experience [*Adam et al*., 1997] shows that the run durations employed (generally 48 h) were sufficient for equilibrium between coexisting fluids and melts to be obtained.

2.4. Sample Preparation and Analysis

After experiments, each capsule was cleaned and weighed before a small opening was made to check for water retention and H_2O-saturation during experiments (if successfully retained, water could be seen to well from of the newly made opening). Although this potentially allows for the preferential loss of some solutes in the escaped fluid (see discussion in *Kessel et al*. [2004]), we have found from previous experience [*Adam et al*., 1997] that any solutes lost in this way are similar in composition to the bulk solute remaining inside capsules. After drying at 110°C, capsules were vacuum impregnated with epoxy before being longitudinally sectioned with a diamond saw. This was done to avoid the potential loss of water-soluble components. The two capsule halves were then reimpregnated with epoxy while being mounted for polishing and analysis. Polished was done using a nonaqueous lubricant.

Major and minor element concentrations in run products were analyzed using two different electron microprobes. These included a Cameca® SX100 and a Zeiss EVO MA15 scanning electron microscope fitted with an X-Max 20 m^2 detector. Although less sensitive than the SX100, the EDS system used in the EVO MA15 was able to analyze broader areas and had less tendency to cause Na_2O and K_2O loss during analyses. Thus, it was more suitable for analyzing the heterogeneous (and delicate) materials produced in our experiments. Operating conditions for the SX100 are described in *Adam and Green* [2006]. For the EVO MA15, the beam was operated at 15 kV and 3 nA, with an acquisition time of 60 s. Data collection and processing was conducted using Oxford Aztec® software. The concentrations of trace and minor elements, together with some major elements, were analyzed with a laser ablation microprobe coupled to an Agilent 7700 series ICP-MS. The spot size varied from 15 μm for crystals to 40 μm diameter for solidified melts and precipitated solutes. During analyses of solutes and melts, the beam was traversed along a 240 μm long track to increase the surface area averaged during each analysis. Other procedures were similar to those used by *Norman et al*. [1996] but employed a mixture of He and Ar to maximize ablation and detection limits. The internal standards used were Ca, Mg, and Al (dependent on the material being analyzed). Data reductions were performed using the GLITTER software program [*van Achterbergh et al*., 2001].

2.5. Accuracy, Precision, and Detection Limits

During each analytical session with the ICP-MS, the international standard BCR-2 was run at regular intervals as a check for accuracy and analytical drift. An average of eight analyses is shown in Table S1 of supporting

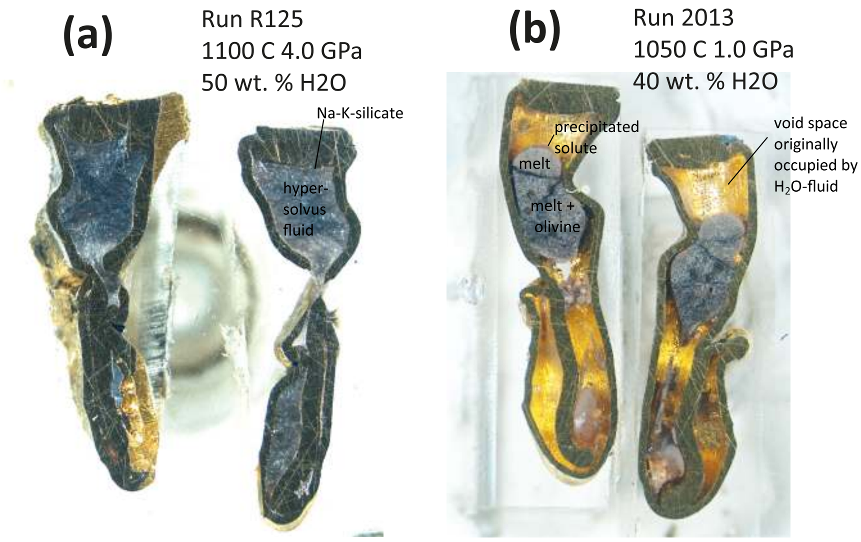

Figure 1. Longitudinal sections of two experimental capsules produced at (a) 4.0 GPa and (b) 1.0 GPa after impregnation with epoxy and polishing. The sections illustrate both the distribution of run products (including aqueous fluids) inside capsules (after quenching) and the strong effect of pressure on the solubility of silicates in aqueous fluids.

information, together with recommended values from GeoRem [see *Jochum et al*., 2007]. During analyses of minerals, the detection limits for rare earths, Th, U, Y, Sr, In, and Cs were <0.1 ppm. For most other elements, they were <1.0 ppm, with values for B, Ti, Zn, and Sn equal to a few ppm or less. Only P and K had higher detection limits equal to several tens of ppm. One sigma uncertainties calculated from counting statistics were typically within ±10% of measured values although typically 2–3 times higher than this for replicate analyses of individual phases.

For the solidified melts and fluid precipitates, the detection limits for most trace elements were <0.1 ppm and in almost all cases <1.0 ppm. One sigma uncertainties for replicate analyses were in most cases similar to those attributable to counting statistics (±10% or less) although significantly larger (by up to several times) for some runs.

2.6. The Calculation of Solute Concentrations in Aqueous Fluids

Total solute concentrations in aqueous fluids were estimated from calculated mass balances between the compositions of starting materials and run products. The mass balances were calculated by constrained least squares regressions performed repetitively during Monte Carlo simulations, allowing us to obtain the full probability distributions for each run (see Appendix A). Trace element concentrations were also included as constraints in these calculations, but in some cases particular elements were not included on account of their propensity for alloying with metal capsules (thereby changing the bulk composition of the starting materials). Bulk fluid compositions and D values for trace elements were simultaneously calculated along with their associated probabilities. Although the results depend on assumed H_2O solubilities in coexisting melts (~10 wt % per GPa), these can be estimated with a reasonable degree of accuracy. The calculated values can also be compared with the direct visual evidence from run products (e.g., Figures 1 and 2).

3. Results

3.1. Description of Run Products

A list of run products and conditions for individual experiments is presented in Table 1. All of the experiments at temperatures ≥1050°C produced either crystallite-rich glass or felt-like masses of feathery crystallites (± glass) that are interpreted as solidified basanite melts (Figures 2a–2d and S1–S12). Coexisting areas are occupied by dispersed mixtures of small white spherules and filamentous crystallites. In some experiments, the spherules have a tendency to adhere to the crystallites in arrangements that are reminiscent of threaded beads (Figures 2a, 2b, and S1–S12). The spherules and crystallites are interpreted as the solutes from aqueous fluids that were precipitated as experiments were quenched. The appearance of the solutes

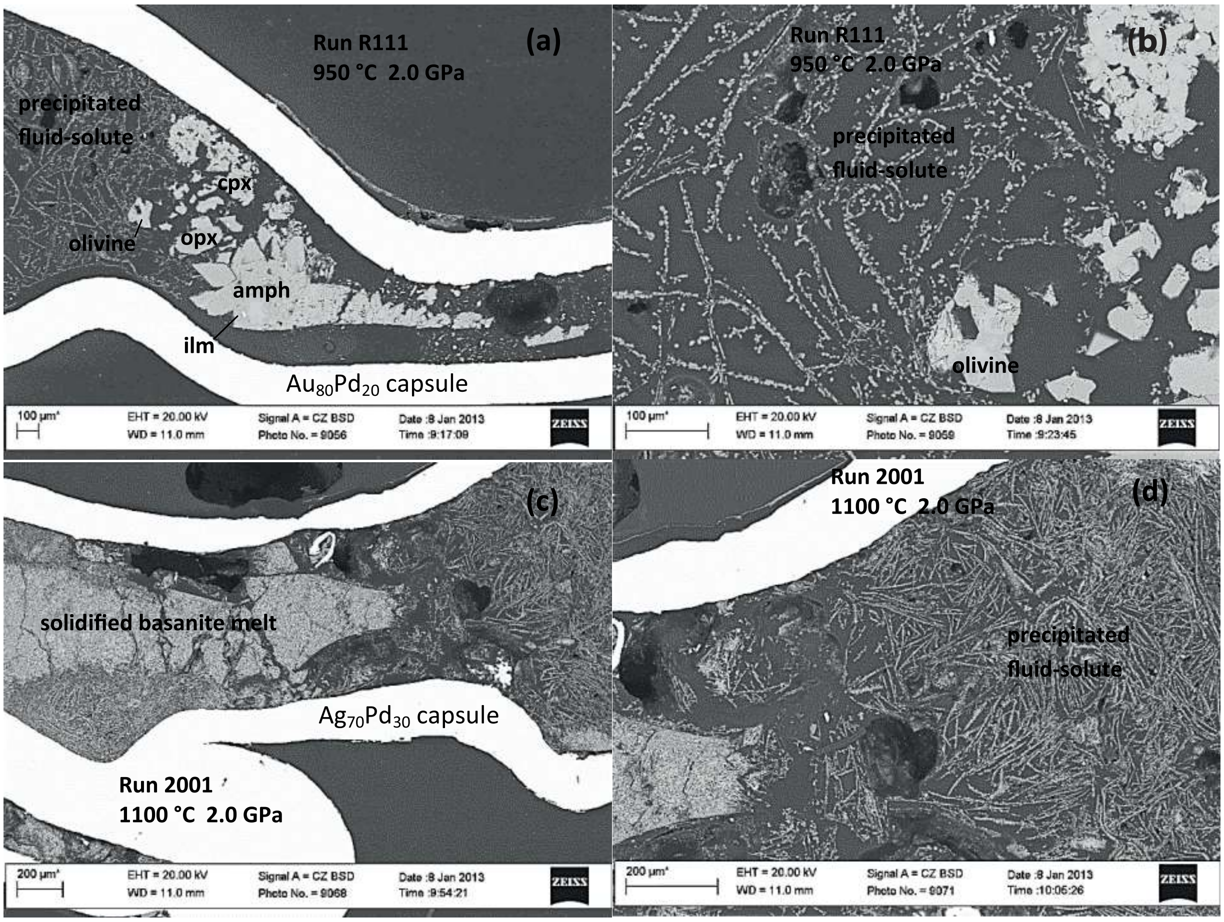

Figure 2. BSE images of solidified melts, precipitated solutes from aqueous fluids, and coexisting mineral phases.

(including their degree of dispersal) varies greatly depending upon the pressure and temperature of each experiment. At the lowest pressure (1.0 GPa), it forms narrow selvages along capsule walls and the boundaries with quenched melts. In these cases, most of the volume originally occupied by the hydrous fluid is now void space (Figure 1a). But at 2.0 GPa, the solute is sufficiently interconnected and dense to be self supporting (Figures 2c and 2d). With increasing pressure, the density and mass of the solute increases, and its

Table 1. Run Products and Conditions for Individual Experiments[a]

Run	wt % H_2O in Starting Mix	Capsule	°C	GPa	Result
1627[b]	40	$Ag_{70}Pd_{30}$	1100	2.0	7 amph + 11 cpx + 1 olivine + 2 spinel + 24 melt + 44 fluid
R111	40	$Au_{80}Pd_{20}$	950	2.0	36 (7) amph + 7 (2) mica + 1.0 (0.5) ap + 0.5 (0.4) ilm + 3 (4) cpx + 0.1 (0.8) opx + 0.1 (0.6) ol + 48.3 (3.5) fluid (+ 3.2 ± 0.7 % FeO loss)
2001	40	$Ag_{70}Pd_{30}$	1100	2.0	3.5 (1.9) ol + 55 (9) melt + 39 (6) fluid (+ 1.2 ± 0.7 FeO loss)
R122	50	Au	1100	3.0	5.9 (0.6) ol + 37 (7) melt + 58 (5) fluid (+2.9 ± 0.2 % FeO loss)
2003	40	$Au_{80}Pd_{20}$	1100	1.0	3.3 (0.8) ol + 45 (2) melt + 43 (2) fluid (+ 6.4 ± 0.1 % FeO loss)
2006	40	$Au_{80}Pd_{20}$	1100	1.0	3 (2) ol + 51 (3) melt + 36 (2) fluid (+6.6 ± 0.1 % FeO loss)
R125	50	Au	1100	4.0	Na-K-silicate + single phase
2013	40	Au	1050	1.0	9.3 (1.0) ol + 51.5 (2.0) melt + 37.0 (1.0) fluid (+ 0.9 ± 0.0% FeO loss)
2014	50	$Au_{80}Pd_{20}$	1200	2.0	39 (5) melt + 57 (3) fluid (+ 2.5 ± 0.4% FeO loss)

[a]Abbreviations include: amph, amphibole; cpx, clinopyroxene; opx, orthopyroxene; ap, apatite; ilm, ilmenite. The estimated modal proportions and FeO-loss were calculated from mass balances between starting materials and run products (see Appendix A). Figures in parentheses are uncertainties (one standard deviation).
[b]Experiment on the Southern Highlands basanite 45065 from Adam and Green [1997].

Table 2. Major and Minor Element Concentrations in Run Products

Method	WDS		WDS		WDS		WDS		WDS		WDS		WDS	
Run	R111		R111		R111		R111		R111		R111		R111	
	opx	1 std n = 3	cpx	1 std n = 6	olivine	1 std n = 3	amph	1 std n = 19	mica	1 std n = 3	ilm	1 std n = 2	solute	1 std n = 12
SiO_2	55.40	0.27	53.38	0.75	39.69	0.33	45.61	2.22	40.19	0.16	0.05	0.00	64.15	4.05
TiO_2	0.18	0.03	0.48	0.17	0.04	0.02	1.28	0.15	1.89	0.01	57.03	0.52	0.94	0.53
Al_2O_3	2.75	0.22	2.46	0.72	0.01	0.00	11.79	2.26	15.61	0.25	0.09	0.02	17.19	1.05
Cr_2O_3	0.45	0.05	0.48	0.14	0.02	0.01	0.21	0.18	0.01	0.02	0.10	0.14	0.02	0.02
FeO	8.41	0.20	4.07	0.32	15.91	2.37	6.66	2.07	7.94	0.35	32.20	2.67	2.07	1.52
MnO	0.40	0.03	0.27	0.10	0.35	0.05	0.21	0.05	0.09	0.00	0.86	0.07	0.06	0.05
NiO	0.02	0.01	0.01	0.01	0.08	0.11	0.01	0.02	0.00	0.01	0.01	0.01	0.04	0.05
MgO	31.53	0.21	17.16	1.06	43.59	2.06	17.82	2.27	20.60	0.35	9.34	1.92	2.30	1.91
CaO	0.76	0.09	21.05	1.23	0.07	0.06	10.66	0.23	0.00	0.01	0.24	0.07	2.17	2.73
Na_2O	0.10	0.00	0.62	0.20	0.07	0.01	2.79	0.12	0.92	0.01	0.09	0.07	5.73	1.17
K_2O	0.00	0.00	0.01	0.02	0.01	0.00	0.91	0.19	8.74	0.06	0.01	0.01	3.79	0.49
P_2O_5	0.02	0.01	0.02	0.01	0.17	0.12	0.04	0.02	0.00	0.00	0.00	0.00	1.55	2.49
Sum	100.00		100.00		100.00		98.00		96.00		100.00		100.00	
Original total	100.74		100.50		100.78		97.79		93.89		100.48		30.24	
Mg no.	87.0		88.3		83.0		82.7		82.2		34.1		66.4	

Method	XRF	EDS		EDS		WDS		WDS		EDS	
Run/Sample	UT-70489	UT-70489		2013		2001		2014		R122	
	Rock	glass	1 std n = 12	melt	1 std n = 8	melt	1 std n = 12	melt		melt	1 std n = 8
SiO_2	44.51	44.44	0.49	46.77	0.26	44.39	1.03	44.23	1.16	45.43	0.27
TiO_2	2.50	2.20	0.67	3.23	0.08	2.72	0.19	2.69	0.29	2.99	0.14
Al_2O_3	11.33	11.10	0.12	13.61	0.26	11.07	0.30	10.46	0.48	11.85	0.15
Cr_2O_3	0.06			0.00	0.00	0.10	0.02			0.15	0.07
FeO	11.96	11.94	0.23	8.80	0.39	11.20	0.83	9.12	0.70	7.38	0.17
MnO	0.19			0.19	0.02	0.23	0.05	0.17	0.07		
NiO	0.05				0.06	0.03			0.06	0.05	
MgO	11.92	12.62	0.47	7.68	0.52	12.51	0.77	17.83	1.38	15.56	0.55
CaO	9.71	9.45	0.09	10.85	0.36	10.07	1.37	9.94	2.56	10.61	0.55
Na_2O	4.14	3.95	0.07	4.88	0.22	5.08	1.49	3.83	0.67	3.12	0.12
K_2O	2.22	2.21	0.07	2.19	0.77	0.89	0.31	0.37	0.12	1.20	0.36
P_2O_5	1.41	1.45	0.23	1.98	0.09	1.71	0.34	1.30	0.02	1.48	0.16
Sum	100.00	99.35		100.00		100.00		100.00		100.00	
Original total				95.06		73.29		78.98			
Mg no.	64.0	65.3		60.9		66.6		77.7		79.0	

Method	WDS		EDS		EDS		WDS		WDS		EDS	
Run	R111		R111		2013		2001		2014		R122	
	solute	1 std n = 12	solute	1 std n = 8	solute	1 std n = 6	solute	1 std n = 12	solute	1 std n = 10	solute	1 std n = 10
SiO_2	64.15	4.05	63.28	0.42	62.20	2.46	55.13	6.67	55.98	2.74	49.79	0.88
TiO_2	0.94	0.53	0.88	0.23	1.24	0.66	1.52	0.61	1.60	0.44	2.28	0.21
Al_2O_3	17.19	1.05	17.57	0.31	17.75	0.91	15.57	1.42	16.47	1.53	12.52	0.70
Cr_2O_3	0.02	0.02	0.11	0.11	0.00	0.00	0.06	0.11			0.14	0.08
FeO	2.07	1.52	2.20	0.22	2.86	0.38	4.49	1.92	4.71	1.33	5.89	0.31
MnO	0.06	0.05	0.08	0.12			0.08	0.04	0.09	0.06	0.16	0.09
NiO	0.04	0.05	0.04	0.12			0.02	0.02			0.03	0.05
MgO	2.30	1.91	1.92	0.42	1.77	1.33	5.20	2.53	0.09	2.40	10.83	0.64
CaO	2.17	2.73	1.25	0.19	2.06	1.82	5.09	2.62	4.35	1.91	8.46	0.78
Na_2O	5.73	1.17	7.51	0.18	6.38	0.43	7.03	7.45	3.26	0.89	5.64	1.00
K_2O	3.79	0.49	5.09	0.38	5.57	0.53	4.67	0.86	5.92	0.86	3.85	0.49
P_2O_5	1.55	2.49	0.07	0.13	0.17	0.41	1.15	0.94	0.63	0.04	0.42	0.26
Sum	100.00		100.00		100.00		100.00		100.00		100.00	
Original total	30.24		30.24		29.42		34.71		30.81		99.67	
Mg no.	66.4		60.9		79.9		67.4		72.6		76.6	
Estimated solute concentration in fluid	19.2	7.3			7.3	2.1	25.0	14.2	25.3	6.0	33.4	7.7

Mg no. = 100 × Mg/(Mg + total Fe) on a molecular basis.
1 std = one standard deviation, n refers to number of replicate analyses.
WDS indicates analysis by wave-length X-ray fluorescence using the Cameca SX100.
EDS indicates analysis by energy dispersive X-ray fluorescence using the Zeiss EVO MA15 and X-Max 20m^2 detector.
All concentrations are in weight percent.
Solute concentrations in fluids were calculated from the results of mass balances between run products and starting materials (see Appendix A).
The 1 sigma uncertainties for oxides are based on the results for replicate analyses of run products n = number of analyses.

Table 3. Fluid/Mineral and Fluid/Melt Partition Coefficients[a]

Run	R111		R111		R111		R111		R111		2003		2006		2013		2001		2014		R122		1627	
GPa	1.0		1.0		1.0		1.0		1.0		1.0		1.0		1.0		2.0		2.0		3.0		2.0	
°C	950		950		950		950		950		1100		1100		1050		1100		1200		1100		1100	
	Fluid/Opx		Fluid/Cpx		Fluid/Olivine		Fluid/Amph		Fluid/ Mica		Fluid/Melt		Fluid/Melt		Fluid/Melt		Fluid/Melt		Fluid/Melt		Fluid/Melt		Fluid/Melt	
	D	Std	D	Std	D	Std	D	Std	D	Std	D	Std	D	Std	D	Std	D	Std	D	Std	D	Std	D	Std
Li7	*1.6*	*0.7*	*3.4*	*1.5*	*1.3*	*0.3*	*5*	*7*	*1.0*	*1.7*	*0.17*	*0.03*	*0.08*	*0.06*	0.04	0.01	*0.7*	*0.1*	1.3	0.6	1	5	*1.8*	*0.2*
Be9	*4.3*	*4.3*	*3.4*	*2.5*			*1.7*	*0.6*	*4.1*	*2.7*	*0.25*	*0.04*	*0.032*	*0.011*	0.06	0.02	*0.08*	*0.00*	0.28	0.08	0.5	0.1	*0.8*	*0.2*
B11	*12*	*12*	*17*	*17*	*12*	*11*	*11*	*11*	*5*	*6*	*0.23*	*0.04*	*0.028*	*0.007*	0.06	0.02	*0.16*	*0.03*	0.2	0.5	1	6	*1.9*	*0.7*
P31	*1.8*	*1.3*	*11*	*7*	*1.4*	*0.4*	*5*	*3*	*5*	*4*	0.04	0.01	0.03	0.02	0.023	0.006	0.27	0.04	0.12	0.03	0.3	0.1	*1.5*	*0.5*
K39											0.9	0.2	0.18	0.14	0.29	0.08	5.9	1.1	7	2	2	44	*11*	*1*
Sc45	0.2	0.1	0.04	0.01	2	61	0.05	0.02	0.5	2.0	0.015	0.003	0.013	0.007	0.007	0.002	0.17	0.02	0.07	0.01	0.50	0.07	*0.86*	*0.08*
Ti47	4	10	1.3	0.6	11	2	0.3	0.1	0.2	0.1	0.11	0.03	0.05	0.03	0.05	0.01	0.36	0.05	0.24	0.08	0.42	0.03	*1.5*	*0.1*
V51	*0.50*	*0.32*	*0.22*	*0.08*	*8*	*3*	*0.13*	*0.05*	*0.13*	*0.05*	*0.65*	*0.17*	*0.06*	*0.03*	0.26	0.09	*0.122*	*0.006*	1.1	0.5	0.34	0.05	*3.7*	*0.3*
Cr53	*0.006*	*0.004*	*0.004*	*0.002*	*0.19*	*0.07*	*0.007*	*0.007*	*0.36*	*0.25*	*0.02*	*0.00*	*0.006*	*0.001*	0.004	0.001	*0.022*	*0.002*	0.08	0.02	0.22	0.12	*0.8*	*0.4*
Mn55	*0.11*	*0.03*	*0.12*	*0.04*	*0.10*	*0.03*	*0.18*	*0.05*	*0.37*	*0.13*	*0.04*	*0.00*	*0.010*	*0.001*	0.011	0.003	*0.040*	*0.001*	0.16	0.04	0.37	0.04	*1.1*	*0.1*
Co59	*0.06*	*0.03*	*0.18*	*0.07*	*0.03*	*0.01*	*0.10*	*0.04*	*0.08*	*0.03*	*0.06*	*0.01*	*0.018*	*0.005*	0.012	0.004	*0.049*	*0.004*	0.24	0.06	0.40	0.06	*1.4*	*0.2*
Ni60	*0.05*	*0.07*	*0.2*	*0.2*	*0.02*	*0.02*	*0.07*	*0.09*	*0.2*	*0.3*	*0.9*	*0.9*	*0.03*	*0.02*	0.008	0.003	*0.044*	*0.004*	0.20	0.05	0.4	3.0	*1.2*	*0.2*
Ni62	*0.07*	*0.07*	*0.26*	*0.25*	*0.02*	*0.02*	*0.11*	*0.11*	*0.26*	*0.25*	*0.5*	*0.3*	*0.06*	*0.05*	0.015	0.009	*0.044*	*0.004*	0.3	0.1	0.7	4.2	*1.2*	*0.3*
Cu63			*13*	*19*			*16*	*24*			*5.8*	*3.3*	*1.6*	*1.0*	0.26	0.11	*0.18*	*0.03*	6	3	1.1	4.9	*1.1*	*0.8*
Cu65							*14*	*20*			*6.6*	*8.1*	*1.5*	*1.1*	0.32	0.16	*0.18*	*0.02*	7	4	0.4	4.3	*1.2*	*0.9*
Zn66	*1.0*	*1.5*	*4*	*6*	*0.68*	*1.10*	*1.23*	*2.09*	*1.51*	*2.38*	*0.4*	*0.3*	*0.04*	*0.03*	0.007	0.003	*0.013*	*0.001*	0.24	0.09	0.0	1.5	*0.9*	*0.2*
Ga69	5	11	5	4			1	2	0.2	0.1	0.22	0.05	0.05	0.04	0.111	0.030	1.04	0.14	0.7	0.3	1.2	0.3	*2.2*	*0.2*
Ga71	5	31	3	4	56	465	0.8	0.5	0.5	0.2	0.4	0.1	0.09	0.06	0.15	0.04	0.86	0.12	0.8	0.4	0.5	0.1	*2.2*	*0.2*
Rb85							19	96	0.1	0.0	0.8	0.4	0.3	0.2	0.53	0.14	4.3	1.3	9	4	0.4	15.7	*15.1*	*1.9*
Sr86			0.8	0.2			0.4	0.3	0.5	0.1	0.028	0.005	0.014	0.008	0.007	0.002	0.42	0.06	0.20	0.06	0.7	0.1	*0.83*	*0.05*
Sr88	240	1266	0.8	0.2	4767	20720	0.4	0.2	0.5	0.1	0.027	0.005	0.014	0.008	0.007	0.002	0.41	0.06	0.21	0.07	1.3	0.1	*0.88*	*0.05*
Y89	0.9	1.4	0.04	0.01	20	119	0.0	0.0	0.5	1.9	0.005	0.001	0.007	0.005	0.002	0.000	0.11	0.02	0.03	0.01	0.4	0.2	*0.28*	*0.03*
Zr90	17	70	1.0	0.5	47	10	0	6	6	81	0.015	0.003	0.014	0.008	0.005	0.001	0.17	0.03	0.07	0.02	0.3	0.1	*0.39*	*0.03*
Nb93	254	2399	245	2488	185	41	3	1	1.8	0.5	0.11	0.03	0.04	0.03	0.04	0.01	0.29	0.04	0.14	0.03	0.5	0.1	0.75	0.07
Mo95			*1.17*	*1.32*					*0.9*	*1.2*	*0.42*	*0.10*	*0.13*	*0.18*	0.62	0.26	*0.10*	*0.05*	1	4	*2.0*	*0.8*		
Ag107											*2.1*	*1.7*	*0.30*	*0.21*	0.02	0.01			10	38	*0.02*	*0.01*	*5*	*1*
Ag109											*1.4*	*1.0*	*0.24*	*0.19*	0.015	0.007			15	122	*0.015*	*0.007*		
Cd111			*1.3*	*1.3*					*1.2*	*1.2*			*0.15*	*0.12*	0.2	0.4	*0.3*	*1.5*	25	840	*0.1*	*2.2*		
In115											*0.9*	*0.6*	*0.18*	*0.09*	0.04	0.02	*0.5*	*2.0*	8	29	*0.2*	*2.7*		
Sn118			*30*	*61*							*1.1*	*0.5*	*0.16*	*0.10*	0.07	0.03	*0.6*	*0.3*	246	4122	0.5	12		
Sb121															0.4	0.3	*0.1*	*0.4*	0.7	0.3	*18*	*14*		
Cs133							38	109	1.0	0.3	1.2	0.6	0.4	0.3	1.0	0.3	4	1	7	3	0.4	4.4	*13*	*2*
Ba137			213	4250			3	18	0.0	0.0	0.031	0.006	0.015	0.009	0.008	0.002	1.7	0.3	0.6	0.3	0.8	4.3	*2.1*	*0.2*
La139	67	317	0.4	0.1	252	964	0.2	0.1	5	75	0.004	0.001	0.007	0.005	0.001	0.000	0.10	0.01	0.04	0.01	0.3	0.2	*0.25*	*0.03*
Ce140	31	58	0.18	0.06			0.11	0.04	3	26	0.004	0.001	0.007	0.005	0.001	0.000	0.09	0.01	0.04	0.02	0.4	0.1	*0.27*	*0.03*
Pr141	15	43	0.10	0.03	70	315	0.07	0.02	3	93	0.005	0.001	0.007	0.004	0.001	0.000	0.10	0.01	0.04	0.02	0.4	0.1	*0.27*	*0.04*
Nd146	8	47	0.07	0.02	40	336	0.05	0.01	0.6	2.2	0.005	0.001	0.007	0.004	0.001	0.000	0.10	0.01	0.03	0.01	0.4	0.2	*0.26*	*0.04*
Sm147	7	53	0.05	0.02	6	27	0.04	0.01	2	24	0.004	0.001	0.007	0.004	0.001	0.000	0.09	0.01	0.03	0.01	0.3	0.1	*0.25*	*0.03*
Eu153	9	72	0.09	0.03	3	7	0.06	0.02	1	6	0.007	0.001	0.008	0.005	0.002	0.001	0.11	0.02	0.05	0.02	0.3	0.2	*0.30*	*0.03*
Gd157	2	16	0.03	0.01			0.03	0.01	1	5	0.006	0.001	0.006	0.004	0.002	0.001	0.11	0.01	0.04	0.02	0.3	0.3	0.25	0.04
Tb159	4	11	0.10	0.05	11	45	0.07	0.03	3	8	0.006	0.001	0.007	0.004	0.002	0.000	0.09	0.01	0.03	0.01	0.3	0.2	0.28	0.04
Dy161	0.7	2.4	0.04	0.01			0.03	0.01	1	10	0.011	0.003	0.008	0.005	0.002	0.001	0.11	0.02	0.05	0.02	0.3	0.2	0.28	0.02
Ho165	3	8	0.05	0.02	2	12	0.04	0.01	1	7	0.005	0.001	0.007	0.004	0.002	0.000	0.11	0.01	0.03	0.01	0.5	0.2	0.24	0.02
Er167	0.8	6.9	0.05	0.02			0.05	0.02	1	4	0.003	0.003	0.005	0.003	0.003	0.002	0.14	0.05	0.25	0.13	0.4	0.1	0.25	0.04
Tm169	22	594	0.3	0.2	9	101	0.3	0.2	7	61	0.005	0.001	0.007	0.004	0.002	0.000	0.11	0.01	0.03	0.01	0.3	0.1	0.29	0.02
Yb173	0.8	0.4	0.12	0.06	6	39	0.1	0.1	3	38	0.013	0.006	0.008	0.005	0.003	0.002	0.10	0.07	0.39	0.20	0.3	0.3	0.29	0.03
Lu175	13	111	1	11	6	22	0.4	0.2	16	93	0.009	0.004	0.012	0.009	0.004	0.002	0.14	0.02	0.06	0.02	0.0	0.3	0.26	0.03
Hf178	4	27	0.5	0.4			0.2	1.5	2	8	0.014	0.003	0.012	0.007	0.005	0.001	0.16	0.02	0.05	0.01	0.3	0.1	0.39	0.03
Ta181	53	228	92	396	115	43	3	2	3	1	0.026	0.005	0.02	0.01	0.012	0.003	0.14	0.03	0.07	0.01	0.5	0.1	0.45	0.03
W182			19	39			25	54	9	19	*0.082*	*0.012*	*0.018*	*0.009*	0.016	0.005	0.08	0.04	0.3	1.1	*2.2*	*1.2*		
Pb208											*1.7*	*1.0*	*0.1*	*0.1*	0.041	0.013	*0.2*	*0.3*	2	3	*1.1*	*0.4*	4.3	1.3
Bi209			*2.7*	*3.0*			*1.9*	*2.1*			*29*	*18*	*0.8*	*0.9*	0.3	0.2	*1*	*29*	15	92	*1.2*	*2.7*		
Th232	55	94	7	83			7	62	2	1	0.005	0.001	0.006	0.004	0.0013	0.0003	0.08	0.01	0.03	0.01	1.0	0.2	0.19	0.02
U238	127	774	10	6			12	128	13	153	0.009	0.002	0.009	0.005	0.0032	0.0008	0.13	0.02	0.05	0.01	0.5	0.2	0.57	0.04

[a]D is the mean partition coefficient and STD the uncertainty calculated as a single standard deviation. Where figures are shown as italics the data for these elements were not used as constraints for the least squares regressions and Monte Carlo simulations (see Appendix A).

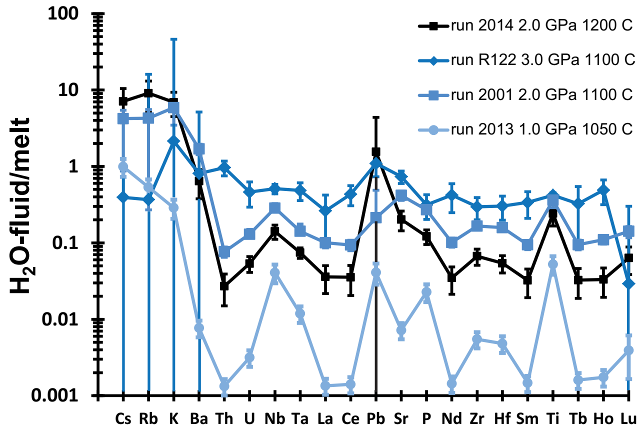

Figure 3. Fluid/melt partition coefficients for lithophile elements in aqueous fluids and basanitic melts. The data are from Table 3 (this study). Error bars are single standard deviations.

appearance increasingly resembles that of the solidified silicate melt (Figures S1–S12). By 4.0 GPa and 1100°C, only a single felt-like matrix is produced (Figures 1a and S12), consistent with complete miscibility between H_2O and the basanite melt.

All of the experiments, except one, produced small amounts of olivine (Run R125 at 4.0 GPa crystallized Na-K-silicate in place of olivine). At 950°C, experiments were either significantly crystalline or subsolidus. One subsolidus experiment at 950°C and 2.0 GPa produced a complete amphibole-mica-ilmenite-lherzolite assemblage, together with an H_2O-rich fluid (Figures 2a and 2b and Tables 1 and 2).

3.2. The Chemical Compositions of Coexisting Fluids, Melts, and Minerals

Analyses of major element concentrations in bulk solutes, melts, and minerals from experiments at 950–1200°C and 1.0–3.0 GPa are given in Table 2. Trace and minor element concentrations analyses by LAM-ICP-MS are provided in Table S2 of supporting information. Fluid/melt and fluid/mineral partition coefficients (D values) are presented in Table 3. H_2O concentrations in the basanitic melts (~10 wt % per GPa) were estimated by combining data for an olivine melilitite at 3.0 GPa [*Brey and Green*, 1977] with solubility measurements for diopside melts at 1.0–3.0 GPa [*Eggler and Burnham*, 1984]. The solute concentrations estimated for aqueous fluids (Table 2) vary from ~7 wt % at 1.0 GPa and 950–1050°C to ~34 wt % at 3.0 GPa and 1100°C (with complete miscibility at 4.0 GPa and 1100°C). They are comparable to values determined by *Schneider and Eggler* [1986] and *Ryabchikov et al*. [1982] who used alternative methods based on the measured weights of recovered run products.

Relative to the basanitic melts produced in experiments, the solutes from coexisting aqueous fluids are enriched in SiO_2, alkalis, Ba, and Pb, but depleted in FeO, MgO, CaO, P_2O_5, and rare earths (REE; Tables 2 and 3 and Figure 3). They are also peralkaline. When H_2O concentrations in the original fluid and melt phases are considered, only the alkalis, Ba, Ag, Bi, and Pb show a consistent preference for the fluid phase (Figures 3 and 4). The solubility of silicates in the aqueous fluid increases rapidly with increasing pressure, with complete miscibility between fluids and melts occurring between 3.0 and 4.0 GPa at 1100°C. Temperature also seems to have a positive effect on solute concentrations in aqueous fluids although this is less obvious than for pressure. Because of these changes, the absolute concentrations of most trace and minor elements in the fluid phase increase with increasing pressure and temperature.

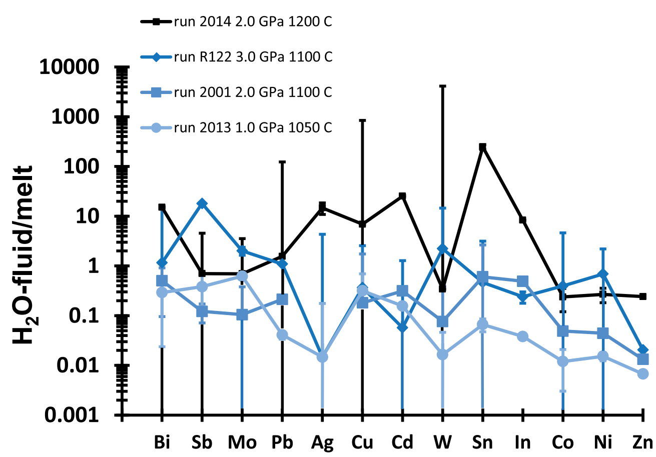

Figure 4. Fluid/melt partition coefficients for chalcophile metals in aqueous fluids and basanitic melts. The data are from Table 3 (this study). Error bars are single standard deviations.

4. Discussion

Two features of the experimental results stand out and are worth

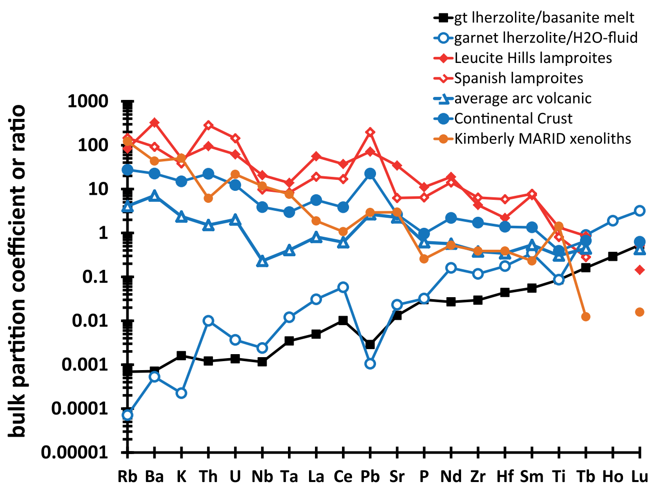

Figure 5. Peridotite/fluid and peridotite/melt partition coefficients for conditions of 2–3 GPa and 1100–1200°C. For comparison, relative incompatible element enrichments in the continental crust, arc volcanics, MARID xenoliths, and lamproites are also shown normalized to the average concentrations in mid-ocean ridge basalts. Data sources include: this work; *Adam and Green* [2011], *Albarede* [2005], *Grégoire et al.* [2002], *Kovalenko et al.* [2010], *Mirnejad and Bell* [2006], *Turner et al.* [1999], and *Wedepohl* [1995].

attention. One is that at ≤1100°C and 1.0 GPa, the capacity of aqueous fluids to transport incompatible elements and economically important metals is low (Figures 3 and 4). In contrast, silicate melts have a much higher capacity. But as pressure and temperature increase, so does the ability of aqueous fluids to transport incompatible elements and metals (Figures 3 and 4). The second feature is the preference of alkalis, Ba, and Pb for aqueous fluids, and the strong preference of REE for silicate melts (Figures 3–5). U is also enriched in fluids relative to Th (Figures 3 and 5). These relationships are consistent with previously published results from experimental studies of fluid partitioning [e.g., *Ayers et al.*, 1997; *Brenan et al.*, 1995a; *Adam et al.*, 1997; *Stalder et al.*, 1998; *Kessel et al.*, 2005b] as well as the essential role that is usually attributed to aqueous fluids during arc magma genesis [e.g., *Tatsumi et al.*, 1986; *Turner et al.*, 1997; *Johnson and Plank*, 1999]. However, the fluid/mineral D values determined in this study (Table 3) are mostly higher than previously published values (Figure 6). This is probably due to our starting composition (which is comparatively rich in Na and K) and the relatively high solubilities of alkali-silicates in aqueous fluids. Thus, total solute concentrations in our experiments were high, with consequential positive effects on the concentrations of trace and minor elements [see *Ayers et al.*, 1997]. Consistent with previous studies [e.g., *Adam et al.*, 1997; *Ayers et al.*, 1997; *Kessel et al.*, 2005a], Nb and Ta are not particularly depleted in aqueous fluids relative to other elements (Figures 3 and 5). Consequently, the Nb and Ta depletions in arc magmas must be the result of residual crystal phases (e.g., rutile) which strongly concentrate both Nb and Ta [see *Brenan et al.*, 1995b; *Xiong et al.*, 2005]. It is also worth noting that most arc magmas are not as strongly enriched in Pb relative to Sr as might be expected from the partitioning relations for H_2O (Figure 5) although this is variable and not evident for the continental crust. It is possible that this reflects some involvement of sulphides in the development of arc magmatism with somewhat different factors contributing to the growth of the continental crust.

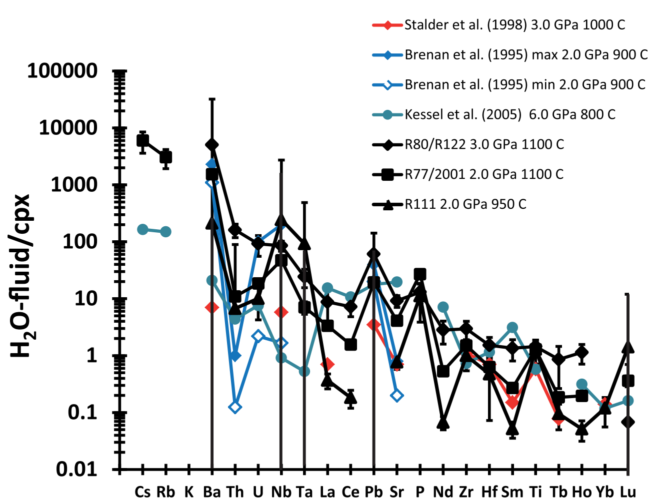

Figure 6. A comparison of fluid/clinopyroxene partition coefficients from this and previously published studies. Data sources include: *Ayers et al.* [1997], *Adam and Green* [2006], *Kessel et al.* [2005b], *Stalder et al.* [1998], and *Brenan et al.* [1995a]. Error bars indicate propagated uncertainties as single standard deviations.

Because the solvent capacities of aqueous fluids are sensitive to pressure and temperature, the ratios of H_2O to some other (nonvolatile) incompatible elements (e.g., Ce) in arc magmas should also be sensitive to the pressures and temperatures of fluid generation. But this will not necessarily be a result of the temperature-dependent solubilities of accessory phases [as suggested by *Plank et al*., 2009]. The pressure-dependent miscibility relations of aqueous fluids and silicate melts also have implications for the second critical end point of the H_2O-saturated peridotite solidus. The latter has been estimated to occur at ~3.8 GPa by two previous studies [*Mibe et al*., 2007; *Gorbachev et al*., 2013]. This contrasts with the value (between 5 and 6 GPa) estimated by *Kessel et al*. [2005a] for a H_2O-basalt system, but is consistent with the closure of the miscibility gap between aqueous fluids and basanitic melts that is observed in our own experiments between 3 and 4 GPa.

Green et al. [2010] proposed that H_2O-fluids can exist in equilibrium with normal mantle peridotite (i.e., the MORB source) at pressures around 6 GPa. But any such fluid will exist above the second critical end point. Thus, it will have qualities intermediate between those normally expected of H_2O-fluids and alkaline silicate melts. Such a fluid will carry K and Ba enrichments, but not the relative Nb, Ta, and Ti depletions characteristic of arc magmas. Consequently, migrating supersolvus fluids are a possible source of the incompatible element enrichments observed in some rocks of deep-seated lithospheric origin, such as Mica-Amphibole-Rutile-Ilmenite-Diopside (MARID; Figure 5). They may also be closely related to the kimberlite and (more particularly) lamproite melts (Figure 5) that bring such samples to the surface.

5. Conclusions

H_2O-saturated experiments on nepheline basanite melts are an indirect means of constraining the nature of aqueous fluids in equilibrium with mantle peridotite. Such fluids are relatively enriched in alkalis, Ba, and Pb compared to coexisting silicate melts. They are also enriched in U relative to Th. These observations are consistent with the essential role usually attributed to aqueous fluids during volcanic arc genesis. But the absolute capacity of H_2O-fluids to transport incompatible elements and economically important metals is a strong positive function of pressure and (to a lesser degree) temperature. Because of this, the relative concentrations of H_2O and other (nonvolatile) incompatible elements in arc magmas should reflect the pressures and temperatures of fluid generation in the subarc environment. At 1100°C and ≤4.0 GPa, complete miscibility occurs between H_2O-fluids and basanitic melts. The supersolvus fluids produced above 4.0 GPa are likely to have properties intermediate between those usually attributed to H_2O-fluids and silicate melts. They will be enriched in K and Ba, but will not have the Nb, Ta, and Ti depletions characteristic of arc magmas. These features are consistent with the incompatible element enrichments found in some mantle xenoliths (e.g., MARID) as well as the lamproite magmas that bring such xenoliths to the surface.

Appendix A

Uncertainties in our reported weight fraction estimates and partition coefficients come from a number of sources. One is the uncertainty of the H_2O concentrations dissolved in melts during experiments. These could not be directed measured but were instead estimated from published solubility data for H_2O in basaltic and related melts. For the purposes of this study, we assumed a one sigma relative uncertainty of ±10% for these values. These uncertainties propagate to our estimated weight fractions of the stable phases, which in turn propagate to the estimation of partition coefficients. Since we expect these uncertainties to be correlated (at least in some cases; Figure A1), traditional analytic methods for error propagation analysis may not be robust. Here we use a Markov Chain Monte Carlo (MCMC) approach to estimate the uncertainties affecting our results. In each iteration *i* of the MCMC simulation, we generate a random sample of the bulk composition vector *d* and phase composition matrix *A* within ±2 standard deviations (σ) of their respective observational uncertainties. This random sample constitutes a trial model drawn from our prior uniform distribution of $\pm 2\sigma$. For each trial, we compute the associated weight fractions of each phase (e.g., Ol, quenched melt, etc) by solving a constrained least square optimization problem [cf. *Gill et al*., 1981].

$$\min \frac{1}{2}\|A_i \cdot x_i - d_i\|_2^2 \tag{A1}$$

subject to the strictly positive constraints

$$x_i \geq x_{low} \tag{A2}$$

Where x_i is the vector (for iteration *i*) containing the weight fractions and x_{low} are the lower limits assumed for the observed phases (here we assumed $x_{low} = 0.001$ for all observed phases). Finally, we compute the

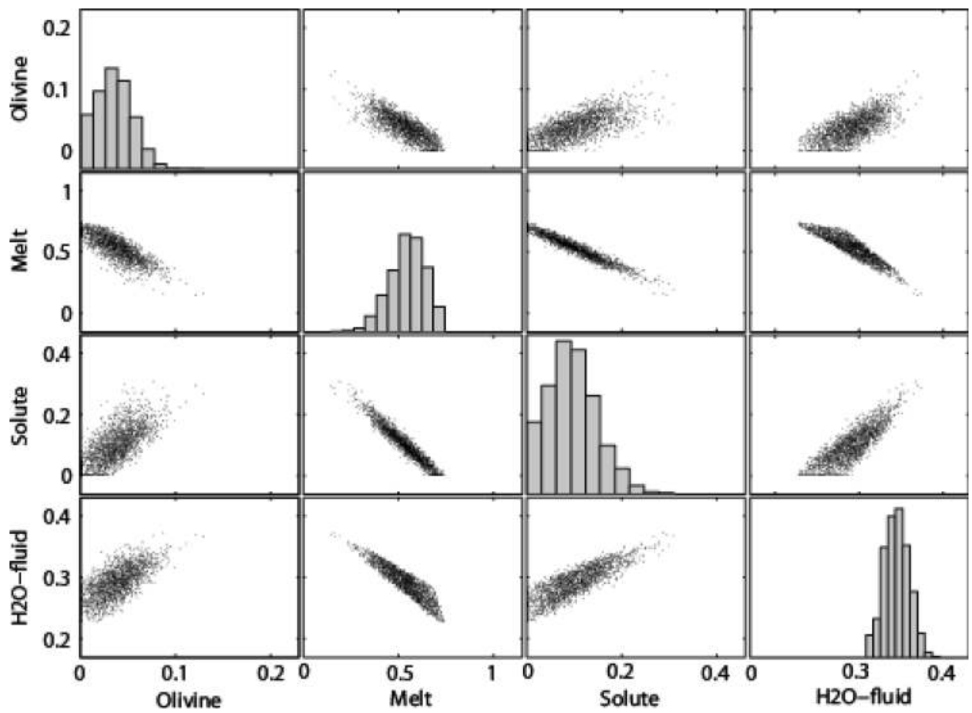

Figure A1. Example of a posterior distribution (run R2001) of weight fractions obtained with the MCMC method described in the Appendix A. The histograms in the diagonals represent the (1-D) marginal posterior distributions for each phase from which mean values and standard deviations can be computed. The nondiagonal plots are point-density representations of 2-D marginals of the posterior distribution. Note the strong correlation between weight fractions (model parameters) for some of the phases (e.g., solute and melt).

partition coefficients D_i as functions of the solution vector x_i. At the end of each iteration, x_i and D_i are either accepted or rejected as part the Markov chain according to a standard Metropolis rule [cf. *Tarantola*, 2005]. To compute the associated probabilities of the vectors x_i and D_i needed by the Metropolis rule, we adopt an objective function (i.e., misfit function) composed of the sum of a L2-norm for major elements and a L1-norm for trace elements [*Tarantola*, 2005]. We choose to use a L1-norm for trace elements due to their large variability and associated uncertainties.

When the above algorithm is iterated many times (here we use 40,000 iterations), we obtain a joint distribution (the full posterior distribution; Figure A1) for *x* and *D* from which standard estimators such as the mean, median, and σ can be evaluated. The later represents the sought uncertainty for our tabulated values.

Acknowledgments
This study was supported by an ARC CCFS grant to M. F. It also made use of instrumentation funded by ARC, LIEF, and DEST Systematic Infrastructure Grants, Macquarie University and Industry. This is contribution 450 from the ARC Centre of Excellence for Core to Crust Fluid Systems (http://www.ccfs.mq.edu.au) and 935 from the GEMOC Key Centre for the Geochemical Evolution and Metallogeny of Continents (http://www.gemoc.mq.edu.au). We gratefully acknowledge the constructive reviews of two anonymous referees.

References

Adam, J. (1990), The geochemistry and experimental petrology of sodic alkaline basalts from Oatlands, Tasmania, *J. Petrol.*, *31*, 1201–1223.

Adam, J., and T. H. Green (2006), Trace element partitioning between mica- and amphibole-bearing garnet lherzolite and hydrous basanitic melt: Experimental results and the investigation of controls on partitioning behaviour, *Contrib. Mineral. Petrol.*, *152*, 1–17.

Adam, J., and T. H. Green (2011), Trace element partitioning between mica- and amphibole-bearing garnet lherzolite and hydrous basanitic melt: 2. Tasmanian Cainozoic basalts and the origins of intraplate basaltic magmas, *Contrib. Mineral. Petrol.*, *161*, 883–899, doi:10.1007/s00410-010-0570-7.

Adam, J., T. H. Green, S. H. Sie, and C. R. Ryan (1997), Trace element partitioning between aqueous fluids, silicate melts and minerals, *Eur. J. Mineral.*, *9*, 569–584.

Albarede, F. (2005), The survival of geochemical heterogeneities, in *Earth's Deep Mantle: Structure, Composition and Evolution, Geophys. Monogr. Ser.*, vol. 160, edited by R. D. van der Hilst et al., pp. 27–46, AGU, Washington, D. C.

Ayers, J. C., and D. H. Eggler (1995), Partitioning of elements between silicate melts and H_2O-NaCl fluids at 1.5 and 2.0 GPa pressure: Implications for mantle metasomatism, *Geochim. Cosmochim. Acta*, *59*, 4237–4246.

Ayers, J. C., and B. Watson (1993), Apatite/fluid partitioning of rare earth elements and strontium: Experimental results at 1.0 GPa and 100 C and applications to models of fluid/rock interaction, *Chem. Geol.*, *107*, 19–22.

Ayers, J. C., S. K. Dittmer, and G. D. Layne (1997), Partitioning of elements between peridotite and H_2O at 2.0–3.0 GPa and 900–1100°C, and application to models of subduction processes, *Earth Planet. Sci. Lett.*, *150*, 381–398.

Bailey, D. K. (1982), Mantle metasomatism—Continuing change within the Earth, *Nature*, *296*, 525–530.

Ballhaus, C., C. G. Ryan, T. P. Mernagh, and D. H. Green (1994), The partitioning of Fe, Ni, Cu, Pt, and Au between sulphide, metal, and fluid phases: A pilot study, *Geochim. Cosmochim. Acta*, *58*, 811–826.

Bodinier, J.-l., C. Merlet, R. M. Bedini, F. Simien, M. Remaidi, and C. J. Garrido (1996), Distribution of niobium, tantalum, and other highly incompatible trace elements in the lithospheric mantle: The spinel paradox, *Geochim. Cosmochim. Acta*, *60*(3), 545–550.

Boyd, F. R., and J. L. England (1960), Apparatus for phase equilibrium measurements at pressures up to 50 kilobars and temperatures up to 1750°C, *J. Geophys. Res.*, *65*(2), 741–748.

Brenan, J. M., H. F. Shaw, F. J. Ryerson, and D. L. Phinney (1995a), Mineral-aqueous fluid partitioning of trace elements at 900°C and 2.0 GPa: Constraints on the trace element chemistry of mantle and deep crustal fluids, *Geochim. Cosmochim. Acta*, *59*, 3331–3350.

Brenan, J. M., H. F. Shaw, D. L. Phinney, and F. J. Ryerson (1995b), Rutile-aqueous fluid partitioning of Nb, Ta, Hf, Zr, U and Th: Implications for high field strength element depletions in island-arc basalts, Earth Planet. *Sci. Lett.*, *128*, 327–339.

Brenan, J. M., F. J. Ryerson, and H. F. Shaw (1998), The role of aqueous fluids in the slab-to-mantle transfer of boron, beryllium, and lithium during subduction: Experiments and models, Geochim. Cosmochim. *Acta*, *66*, 3109–3123.

Brey, G., and D. H. Green (1977), Systematic study of liquidus phase relations in olivine melilitite at high pressures and petrogenesis of an olivine melilitite magma, *Contrib. Mineral. Petrol.*, *61*, 141–162.

Eggler, D. H., and C. W. Burnham (1984), Solution of H_2O in diopside melts: A thermodynamic model, *Contrib. Mineral. Petrol.*, *85*, 58–66.

Fiorentini, M. L., and S. W. Beresford (2008), Role of volatiles and metasomatized subcontinental lithospheric mantle in the genesis of magmatic Ni-Cu-PGE mineralization: Insights from insitu H, Li, B analyses of hydromagmaic phases from Valmaggia ultramafic pipe, Ivrea-Verbano Zone (NW Italy), *Terra Nova*, *20*, 333–340, doi:10.1111/j.1365-3121.2008.00825.x.

Gill, P. E., W. Murray, and M. H. Wright (1981), *Practical Optimization*, Academic, London.

Gorbachev, N. S., A. N. Nekrasov, A. V. Kostyuk, and D. M. Sultanov (2013), Experimental study of melting, texture, and phase relations of basalt (eclogite)-peridotite-fluid system at sub- and supercritical P-T. Abstract, Goldschmidt Conference, *Min. Mag.*, *77*, 1125–1238, doi: 10.1180/minmag.2013.077.5.7.

Green, D. H. (1976), Experimental testing of ''equilibrium'' partial melting of peridotite under water-saturated, high-pressure conditions, *Can. Mineral.*, *14*, 255–268.

Green, D. H., W. O. Hibberson, I. Kovacs, and A. Rosenthal (2010), Water and its influence on the lithosphere-asthenosphere boundary, *Nature*, *467*, 448–451.

Green, T. H. (1973), High-pressure crystallization of an island arc calcalkaline andesite, in *The Western Pacific: Island Arcs, Marginal Seas, Geochemistry*, edited by P. J. Coleman, pp. 497–502, Univ. of West. Aust. Press, Perth, Australia.

Green, T. H., and J. Adam (2003), Experimentally determined trace element characteristics of aqueous fluid from partially dehydrated mafic oceanic crust at 3.0 GPa, 650–700 C, *Eur. J. Mineral.*, *15*, 815–830, doi:10.1127/0935-1221/2003/0015-0815.

Green, T. H., A. E. Ringwood, and A. Major (1966), Friction effects and pressure calibration in a piston-cylinder apparatus at high pressure and temperature, *J. Geophys. Res.*, *71*(14), 3589–3594.

Grégoire, M., D. R. Bell, and A. P. Le Roex (2002), Trace element geochemistry of phlogopite-rich mafic mantle xenoliths: Their classification and their relationships to phlogopite-bearing peridotite and kimberlites revisited, *Contrib. Mineral. Petrol.*, *142*, 603–625.

Hirose, K. H., and T. Kawamoto (1995), Hydrous partial melting of lherzolite at 1 GPa: The effect of H_2O on the genesis of basaltic magmas, *Earth Planet. Sci. Lett.*, *133*, 463–473.

Jochum, K. P., U. Nohl, K. Herwig, E. Lammel, B. Stoll, and A. W. Hofmann (2007), GeoReM: A new geochemical database for reference materials and isotopic standards, *Geostand. Geoanal. Res.*, *29*(3), 333–338.

Johnson, M. C., and T. Plank (1999), Dehydration and melting experiments constrain the fate of subducted sediments, *Geochem. Geophys. Geosyst.*, *1*(12), 1007, doi:10.1029/1999GC000014.

Keppler, H. (1996), Constraints from partitioning experiments on the compositions of subduction-zone fluids, *Nature*, *380*, 237–240.

Kessel, R., P. Ulmer, T. Pettke, M. W. Schmidt, and A. B. Thompson (2004), A novel approach to determine high-pressure high-temperature fluid and melt compositions using diamond-trap experiments, *Am. Mineral.*, *89*, 1078–1086.

Kessel, R., P. Ulmer, T. Pettke, M. W. Schmidt, and A. B. Thompson (2005a), Experimental determination of phase relations and second critical endpoint in K-free eclogite-H_2O at 4–6 GPa and 700–1400°C, *Earth Planet. Sci. Lett.*, *237*(3), 873–892.

Kessel, R., M. W. Schmidt, P. Ulmer, and T. Pettke (2005b), Trace element signature of subduction-zone fluids, melts and supercritical liquids at 120–180 km depth, *Nature*, *437*, 724–727, doi:10.1038/nature03971.

Kovalenko, V. I., V. B. Naumou, A. V. Girnis, V. A. Dorofeeva, and V. V. Yarmolyuk (2010), Average composition of basic magmas and mantle sources of island arcs and active continental margins estimated from data on melt inclusions and quenched glasses of rocks, *Petrology*, *18*(1), 1–26.

Loyd, F. E., and D. K. Bailey (1975), Light element metasomatism of the continental mantle: The evidence and the consequences, *Phys. Chem. Earth*, *9*, 389–416.

Melzer, S., M. Gottschalk, and W. Heinrich (1998), Experimentally determined partitioning of Rb between richterites and aqueous (Na, K)-chloride solutions, *Contrib. Mineral. Petrol.*, *133*, 315–328.

Mibe, K., M. Kanzaki, T. Kawamoto, K. N. Matsukage, Y. Fei, and S. Ono (2007), Second critical endpoint in the peridotite-H_2O system, *J. Geophys. Res.*, *112*, B03201, doi:10.1029/2005BJ004125.

Mirnejad, H., and K. Bell (2006), Origin and source of the Leucite Hills Lamproites: Evidence from Sr-Nd-Pb-O isotopic compositions, *J. Petrol.*, *47*(12), 2463–2489.

Nielson, J. E., and J. S. Noller (1987), Processes of mantle metasomatism; constraints from observations of composite peridotite xenoliths, in *Mantle Metasomatism and Alkaline Magmatism*, Geol. Soc. Am. Spec. Publ., vol. 215, edited by E. M. Morris and J. D. Pasteris, pp. 61–76, Geol. Soc. of Am., Boulder, Colo.

Norman, M. D., N. J. Pearson, A. Sharma, and W. L. Griffin (1996), Quantitative analysis of trace elements in geological materials by laser-ablation ICP-MS: Instrumental operating conditions and calibration values of NIST glasses, *Geostand. Newsl.*, *20*, 247–261.

O'Reilly, S. Y., and W. L. Griffin (1988), Mantle metasomatism beneath western Victoria, Australia: I. Metasomatic processes in Cr-diopside lherzolites, *Geochim. Cosmochim. Acta*, *52*, 433–447.

Plank, T., L. B. Cooper, C. E. Manning (2009), Emerging thermometers for estimating slab surface temperatures, *Nat. Geosci.*, *2*, 611–614.

Ryabchikov, I. D., W. Schreyer, and K. Abraham (1982), Compositions of aqueous fluids in equilibrium with pyroxenes and olivine at mantle pressures and temperatures, *Contrib. Mineral. Petrol.*, *79*, 80–84.

Saunders, A. D., and J. Tarney (1979), The geochemistry of basalts from a back-arc spreading centre in the East Scotia Sea, *Geochim. Cosmochim. Acta*, *43*, 555–572.

Schneider, M. E., and D. H. Eggler (1986), Fluids in equilibrium with peridotite minerals: Implications for mantle metasomatism, *Geochim. Cosmochim. Acta*, *50*, 711–724.

Stalder, R., S. F. Foley, G. P. Brey, and I. Horn (1998), Mineral-aqueous fluid partitioning of trace elements at 900–1200°C and 3.0–5.7 GPa: New experimental data for garnet, clinopyroxene, and rutile, and implications for mantle metasomatism, *Geochim. Cosmochim. Acta*, *62*, 1781–1801.
Tarantola, A. (2005), *Inverse Problem Theory and Model Parameter Estimation*, Soc. for Ind. and Appl. Math., Philadelphia, Pa.
Tatsumi, Y., D. L. Hamilton, and R. W. Nesbitt (1986), Chemical characteristics of fluid phase released from a subducted lithosphere and origins of arc magmas: Evidence from high-pressure experiments and natural rocks, *J. Volcanol. Geotherm. Res.*, *29*, 293–309.
Turner, S., S. Turner, C. Hawkesworth, N. Rogers, J. Bartlett, T. Worthington, J. Hergt, and I. Smith (1997), ^{238}U-^{230}Th disequilibria, magma petrogenesis, and flux rates beneath the depleted Tonga-Kermadec island arc, *Geochim. Cosmochim. Acta*, *61*(22), 4855–4884.
Turner, S., J. P. Platt, R. M. M. George, S. P. Kelley, D. G. Pearson, and G. M. Nowell (1999), Magmatism associated with orogenic collapse of the Betic-Alboran Domain, *J. Petrol.*, *40*(6), 1011–1036.
van Achterbergh, E., C. G. Ryan, S. E. Jackson, and W. L. Griffin (2001), Data reduction software for LA-ICP-MS: Appendix, in *Laser Ablation-ICP-Mass Spectrometry in the Earth Sciences: Principles and Applications, Short Course Ser.*, vol. 29, edited by P. Sylvester, pp. 239–243, Mineralog. Assoc. Canada, Ottowa, Ont.
Wedepohl, K. H. (1995), The composition of the continental crust, *Geochim. Cosmochim. Acta*, *59*, 1217–1232.
Xiong, X. L., J. Adam, and T. H. Green (2005), Rutile stability and rutile/melt HFSE partitioning during partial melting of hydrous basalt: Implications for TTG genesis, *Chem. Geol.*, *218*, 339–359.